Signal Processing and Renewable Energy

March 2023, (pp. 41-55)
ISSN: 2588-7327
eISSN: 2588-7335

Indoor Vehicular Navigation using IMU and LiDAR with EKF Parameters Optimization using Grey Wolf Algorithm

Farshad Khalafian [1*]

[1] Department of Electrical Engineering, Ahvaz Branch, Islamic Azad University, Ahvaz, Iran.

Received: 07-Jul-2022, Revised: 17-Aug-2022, Accepted: 12-Oct-2022.

Abstract

Nowadays, vehicles must be able to localize themselves in all environments, including urban areas and indoor environments where the performance of Global Navigation Satellite Systems (GNSS) may be reduced. In the studies conducted so far in urban environments, an inertial measurement unit (IMU) and an extended Kalman filter (EKF) have been presented. For indoor environments, a light and range detection system (LiDAR) has been developed, which was more accurate than previous methods. However, the accuracy of diagnosis should be improved by providing newer methods .Therefore, in this article, in order to increase the accuracy of the position error of the internal navigation system, an integrated developed IMU/LiDAR Kalman filter was used, and then by optimizing the parameters of the Kalman filter and the gray wolf meta-heuristic algorithm, an attempt was made to reduce the position error. In order to check the performance of the presented method, the results before using the optimization algorithm and after the optimization were evaluated using three different paths. The obtained results, including position, speed, and direction show that the accuracy of the results increases by using the gray wolf algorithm compared to the conventional model.

Keywords: Indoor Vehicular Navigation, IMU/LiDAR, Extended Kalman Filter (EKF), Grey Wolf optimization.

1. INTRODUCTION

The ability to self-localize is essential for many mobile systems, including autonomous vehicles, virtual reality setups, and domestic robots [1]. Such systems have many applications including entertainment, delivery services, and emergency response. These systems use the knowledge of their location to perform tasks like avoidance of dangerous situations, navigation to

*****Corresponding Authors Email: khalafian@iauahvaz.ac.ir

objectives, and mapping of unknown areas. A Global Navigation Satellite System (GNSS) is a powerful tool for localization involving communication between a receiver and satellites in Medium Earth orbit (MEO) [2]. In urban environments where GNSS is mostly available, GNSS, an exteroceptive system, is often fused with Inertial Navigation Systems (INS), which use proprioceptive sensors that measure linear and angular motion of a platform. In indoor navigation where GNSS is unavailable, common sensor setups are used including Light Detection and Ranging (LiDAR) and/or cameras as exteroceptive components and Inertial Measurement Units (IMUs) and/or wheel odometry as proprioceptive components [3]. Radio Detection and Ranging (radar) sensors as exteroceptive point cloud scanners are a relatively new development with unique characteristics compared to LiDAR technology.

To address the urban and indoor localization problem, fusion of both exteroceptive and proprioceptive sensors is necessary and effective for several reasons. Exteroceptive sensors receive information from the environment to perform localization using targets with known poses, resulting in low drift estimations in many situations. They can also be used to recognize areas that have been seen before and use this information to improve the pose trajectory estimate. This use of exteroceptive sensors to learn and recognize the environment is known as Simultaneous Localization and Mapping (SLAM) which is a very effective method for localization. Proprioceptive sensors do not depend on the environment and, in the case of IMUs, can provide pose data in any situation. These sensors use dead reckoning to determine pose, which results in drift over time.

Therefore, proprioceptive sensors are best used for short-term localization data, and exteroceptive sensors are best used for periodic accurate localization and mapping corrections. The complementary effect of both types of sensors allows for a well performing localization system in favorable conditions. Current state of the art autonomous vehicles emphasize the reliance on a fusion of imperfect sensors since there is no single ideal sensor for every situation, and therefore primarily use a combination of LiDAR, radar, GNSS, IMU, and vision [4].

The rest of this paper is organized as follows: Section 2 gives the workflow of Indoor Localization and Navigation methods. Section 3 presents the LiDAR/IMU integrated system using optimal EKF and describes the mathematic principle of the proposed method; Section 4 presents the test results and discusses the results; conclusions are drawn in Section 5.

2. INDOOR LOCALIZATION AND NAVIGATION METHODS

2.1. Indoor Localization

In indoor settings, LiDAR scanners are common sensors used in localization without GNSS. 2D LiDAR scanners are commonly used for ground vehicles due to their reduced cost and complexity. However, 2D LiDAR systems also perform poorly under certain circumstances, such as in environments where limited distinguishable geometry exists like in long corridors (Figure 1).

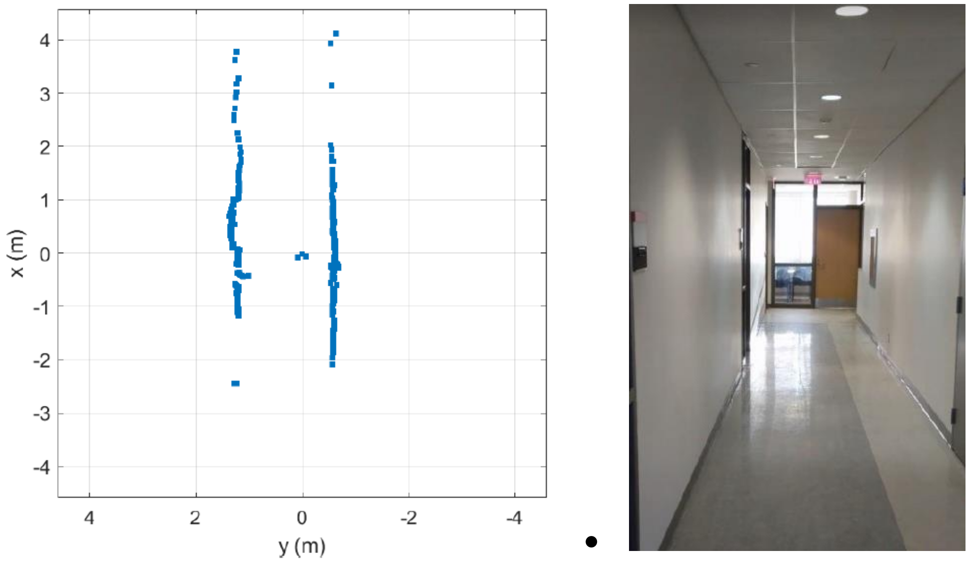

Fig. 1. Long hallway where short range LiDAR detects parallel straight lines.

Because 2D LiDAR scans detect most solid objects on a horizontal plane, a hallway appears as points arranged in two parallel lines. Scan matching with such features results in poor performance [5].

In another article, it was proposed a fingerprint-based indoor localization method, named FPFE (fingerprint feature extraction), to locate a target device (TD) whose location is unknown. in this method Bluetooth low energy (BLE) beacon nodes (BNs) are deployed in the localization area to emit beacon packets periodically. The experimental results show that FPFE achieves an average error of 0.68 m, which is better than those of other related BLE fingerprint-based indoor localization methods [6].

In the article [7] the Kalman Filter-Based Data Fusion of Wi-Fi RTT and PDR for Indoor Localization is used. Firstly, an adaptive filtering system consisting of multiple Extended Kalman Filter (EKF) and a new outlier detection method is proposed to reduce the localization error of Wi-Fi RTT. Secondly, the fusion algorithm based on the Federated Filter (FF) and observability is designed to combine Wi-Fi RTT with PDR. Finally, to further improve the localization performance of the fusion algorithm, a real-time smoothing method with fixed interval is used. The results show that the proposed indoor localization method has better stability and robustness, and the average localization error decreased by 37.4-67.6% compared with the classic EKF-based method.

In reference [8], Smartphone-based indoor localization techniques are presented. Smartphone is now undeniably essential and a very functional tool for everyone. As the need for more powerful computations, faster communications, and more sophisticated location-based services, the number of powerful embedded sensors also becomes indispensable in smartphones. This article explores the sensing capabilities of different smartphone sensors and how they become more functional in the context of wireless-based localization. It identifies the different techniques for efficient indoor localization using the modalities inherent in smartphones. A taxonomy based on the notable approaches used in the system such as mapping, path loss prediction, and dead reckoning is also defined. The strengths and weaknesses of each system and identification and comparison of the technologies used are highlighted. Finally, open issues and challenges for future works are presented.

In [9] a method is proposed using multi-view variational deep learning with application to practical indoor localization. This article introduces a view-selective deep learning (VSDL) system for indoor localization using CSI of WiFi. The multi-view training with CSI obtained from multiple groups of access points (APs) generates latent features on a supervised variational deep network. This information is then applied to an additional network for dominant view classification to minimize the regression loss of localization. As noninformative latent features from multiple views are rejected, we can achieve a localization accuracy of 1.28 m, which outperforms by 30% the best known accuracy in practical applications in a complex building environment.

The matching results from using this geometry only provide localization confidence in the direction perpendicular to the hallway. Wheel odometry or Inertial Measurement Unit (IMU) dead reckoning is often used to aid in these systems when the exteroceptive sensors fail, and therefore can provide estimates along the uncertain dimensions. However, such dead reckoning systems have their own sources of uncertainty that accumulate the longer traversal of the environment continues without updates from external measurements.

2.2. Inertial Measurement Unit (IMU)

Micro-Electromechanical Systems (MEMS) IMUs are widely used motion sensors due to their low cost, low power, and small form factor. Most importantly, the fact that IMUs are completely proprioceptive and do not need any contact or transmission from the external world makes them an attractive technology. They are often used in most mobile systems for their ability to calculate attitude and pose with low resource cost.

IMUs measure accelerations and rates of rotations using accelerometers and gyroscopes, respectively. Sensing these motions is done using Newton’s first law of motion, which states that an object’s acceleration is proportional to the applied external forces on the object. In MEMS IMU sensors, an accelerometer uses a mass connected to a method of suspension with the displacement of the mass indicating the force (which is proportional to acceleration) applied in the direction along the suspension. Gyroscopes measure rates of rotations using the same concept applied to vibrating masses affected by Coriolis forces [10].

MEMS IMUs suffer from a high degree of error, including biases, scale factors, cross-coupling, and random noises. Without accurately characterizing these errors, the use of IMUs to estimate pose is often extremely limited in effectiveness due to the double integration necessary to calculate position from acceleration. Methods for characterizing IMU errors have been developed to correct this issue, including use of Gauss-Markov (GM) random processes and Allan Variance (AV) techniques. The current approach of using these techniques is to generate long records of static measurements to obtain modelling parameters [11-12]. However, these methods do not handle disturbances or changes in the environment and may not result in accurate tuning for practical dynamic motions. In general, pose estimates are accurate within a few seconds, but errors quickly grow unbounded to hundreds of meters in a few subsequent seconds. Therefore, IMUs are often good with estimating pose in the short term but cannot be relied upon in the long term.

The current literature contains several attempts to estimate movement smoothness using data from IMUs, many of which assume that the translational and rotational kinematics measured by IMUs can be directly used with the smoothness measures spectral arc length (SPARC) and log dimensionless jerk (LDLJ-V). However, there has been no investigation into the validity of these approaches. [13-14], But Authors In [15], systematically evaluated the use of these measures on the kinematics measured by IMUs. They demonstrated that the accuracy of LDLJ-A depends on the time profile of IMU orientation reconstruction error.

2.3. Light Detection and Ranging (LiDAR)

LiDAR sensors send out beams of light and measure reflections to create 2D or 3D scans. They are often used to make high-resolution 3D maps for land surveying, geology, forestry, and navigation. LiDAR sensors are often known for being powerful technology with a large price tag and complex mechanical structure. However, recent developments have produced cheaper designs with similar characteristics to high end systems, making them more accessible to a wider audience [16].

LiDAR emits ultraviolet, visible, or near infrared light in a beam commonly steered by rotating mirrors. These beams can detect most materials at very high resolutions, resulting in a system that is able to map physical structures at a centimeter level resolution. By measuring the difference in time between transmitting and receiving a beam, the distance travelled by the beam can be determined. By measuring the angle of the rotating mirrors with rotary encoders at the time of reception, the direction of the beam can be recovered with high angular resolution. The output of LiDAR scanners is typically point cloud data, which represents 3D or 2D points for every beam emitted in one cycle of the mirror rotations [17].

LiDAR as a navigation tool suffers from issues such as being obstructed by rain, aerosols, and dust. Furthermore, moving components pose more risk for mechanical failure and wear and tear. In summary, LiDAR sensors have high potential in being an accurate source of localization data in many environments but cannot be relied upon for every situation yet. Authors in [18] evaluated Lidar for Autonomous Driving. This article presents a review of state-of-the-art automotive lidar technologies and the perception algorithms used with those technologies. Lidar systems are introduced first by analyzing such a system's main components, from laser transmitter to beam-scanning mechanism. The advantages/ disadvantages and the current status of various solutions are introduced and compared. Then, the specific perception pipeline for lidar data processing is detailed from an autonomous vehicle perspective. The model-driven approaches and emerging deep learning (DL) solutions are reviewed. Finally, provided an overview of the limitations, challenges, and trends for automotive lidars and perception systems.

3. PROPOSED METHOD

3.1. IMU/LIDAR System

The mathematical model of the traditional sequential integrated LiDAR/IMU system is shown in Figure 2. The IMU can calculate position (r^n_{IMU}), velocity (V^n_{IMU}), and attitudes (C^n_{bIMU}) using a mechanized algorithm, when no LiDAR observation information is received. The North, East, and Lower Local Area Frame (NED), called the n-frame navigation frame, is used as a reference framework for inertial navigation. The b-frame is defined in the center of the IMU, and the axes are forward, straight, and down, respectively. In fact, the IMU output contains errors, and errors cause navigation results to change rapidly over long periods of time. Therefore, an error propagation model should work alongside the system motion model to further correct and obtain better navigation results. The error state vector in n-frame is defined as follows [19]:

$$\delta x(t) = [(\delta r^n_{IMU})^T (\delta v^n_{IMU})^T \epsilon^T b_g^T b_a^T] \qquad (1)$$

where the error state δx consists of the errors of position (δr^n_{IMU}), the errors of velocity (δv^n_{IMU}), the errors of attitude (ϵ), the bias of gyroscope (bg), and the bias of acceleration (ba), which is a 15-dimension vector.

The biases of gyroscope and accelerometer are modeled as a first-order Gauss-Markov process with correlation time T and mean square value σ^2. The model is described by:

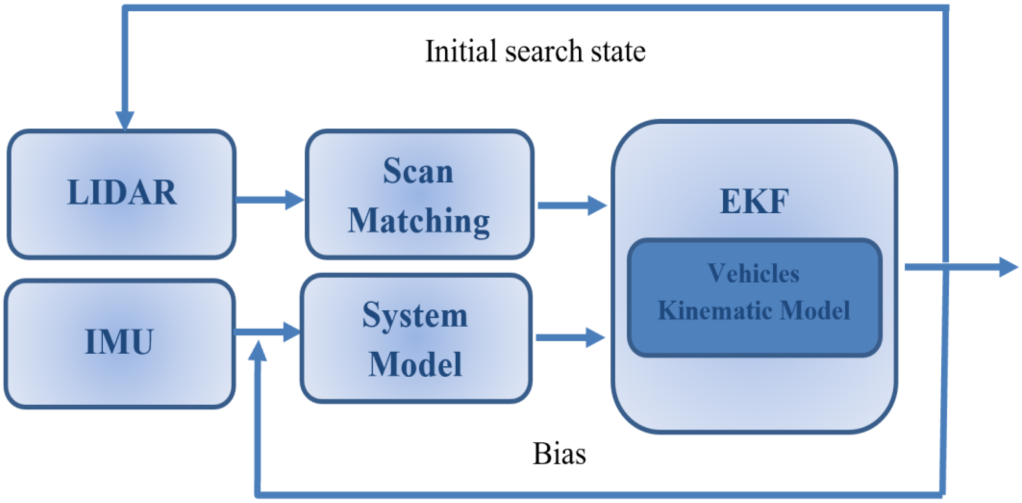

Fig. 2. System architecture diagram of the estimation of navigational solution based on LiDAR/IMU.

$$\dot{b}_g(t) = -\frac{1}{T_{gb}} b_g(t) + \omega_{gb}(t) \qquad (2)$$

$$\dot{b}_a(t) = -\frac{1}{T_{ab}} b_a(t) + \omega_{ab}(t) \qquad (3)$$

In equations (2) and (3), the bias of gyroscope (bg), and the bias of acceleration (ba), correlation time T, and ω is the forcing vector of white noise. The INS error model with the sensor error models in continuous time can be expressed by

$$\delta x\dot{(t)} = F(t)\delta x(t) + G(t)\omega(t) \qquad (4)$$

F is the dynamic matrix, G is a noise-input mapping matrix, and ω is the forcing vector of white noise, according to the system motion model and concrete formation of F, G that can be found in the works of Shin, 2001 and 2005 [20, 21]. The discrete form of (4) is:

$$\emptyset_{k/k-1} = \exp(F(t_k)\Delta t) \approx I + F(t_k)\Delta t \quad (5)$$

In the above relationship $wk{-}1$ is a sequence of zero-mean random variable and covariance matrix associated with wk is given by:

$$E\left[w_k w_j^T\right] = \{\begin{matrix} 0 & k = j \\ Q_k & k \neq j \end{matrix} \qquad (6)$$

$$Q_k \approx \emptyset_k G(t_k) Q G(t_k)^T \emptyset^T \Delta t \qquad (7)$$

$$Q = diag(vrw^2, arw^2, \frac{2\sigma_{gb}^2}{T_{gb}}, \frac{2\sigma_{ab}^2}{T_{ab}}) \qquad (8)$$

Qk is the covariance matrix; Q is the spectral density matrix; vrw and arw are velocity random walk and angular random walk, which are given by the IMU user manual; T_{gb} and T_{ab} are the correlation times of gyroscopes and accelerometers, respectively; $\sigma^2{}_{gb}$ and $\sigma^2{}_{ab}$ are the mean square values of gyroscopes and accelerometers.

3.2. EKF Parameter Tuning

The IMU/LIDAR EKF system contains both parameters that are approximately measurable and parameters that are completely unknown. The process covariance matrix for instance, commonly denoted Q, contains the random walk error of the IMU sensors, which can be estimated through certain modelling techniques but cannot be calculated optimally. The measurement noise covariance matrix, denoted R, is unknown and can often only be tuned in a manual trial and error method. These matrices are of high importance since they directly impact the degree to which the filter favors one sensor reading over another, and small variations in some values may result in a complete divergence in the estimation. Therefore, optimal tuning of these matrices is strongly desired.

The LiDAR and IMU measurements are fused by the EKF algorithm only at the epoch in which LiDAR scan information is obtained. The EKF observation functions are given briefly:

$$z_k = [\begin{matrix} r_{IMU}^n & r_{LiDAR}^n \\ \epsilon_{IMU}^n & \epsilon_{LiDAR}^n \end{matrix}] = H_k \delta x_k + v_k) \qquad (9)$$

where z_k is a 4-dimensional measurement vector; $r^n{}_{\mathrm{IMU}}$ is the predicted position from the IMU mechanization; $r^n{}_{\mathrm{LiDAR}}$ is the observed position from LiDAR; $\epsilon^n{}_{\mathrm{IMU}}$ and $\epsilon^n{}_{\mathrm{LiDAR}}$ are the predicted and observed heading angles, respectively, which are expressed as Euler angles. They make up the four observations. Hk is the designed matrix that describes the relation between the state vector and the measurements and is given in (10); Vk is the driven response of the input white noise at time (k+1). The measurement covariance matrix is written as:

$$\delta x_{k=1}^{-} E\left[v_k v_j^T\right] = \{ \begin{matrix} 0 & k = j \\ R_k & k \neq j \end{matrix} \qquad (10)$$

$$R_k = diag(\delta_r^2, \delta_c^2) \qquad (11)$$

R_k is a 4-dimension covariance matrix. δr, $\delta \epsilon$ are the errors of position and heading, which approximate values based on the properties of the laser scanner device, and the angle and range searching intervals of the LiDAR scan matching algorithm. The estimates of the EKF prediction functions are:

$$\delta x_{k+1}^{-} = \emptyset_k \delta x_k \qquad (12)$$

$$P_{k+1}^{-} = \emptyset_k P_k \emptyset_k^T + Q_k \qquad (13)$$

The Kalman gain is:

$$K_k = P_k^{-} H_k^T (H_k P_k^{-} H_k^T + R_k)^{-1} \qquad (14)$$

The state vector is updated as:

$$\delta x_k = \delta x_k^{-} + K_k(z_k - H_k \delta x_k^{-} \qquad (15)$$

$$P_k = (I - K_k H_k) P_k^{-} \qquad (16)$$

where $\delta x - k$ and $P - k$ are the prior estimate and its error covariance. The P matrix, namely, the estimated standard deviations of the estimated states.

3.3. EKF Parameter Optimization using GWO

Meta-heuristic algorithm is one of the optimizing techniques. It is inspired by the principles or structures of nature and is used to solve optimization problems [22-24]. In the past 20 years, the optimization algorithm has received extensive attention and has been well developed. After all, it is a new type of optimization method, and can describe all aspects of nature to create a different optimization model. There are many aspects in this area, such as particle swarm optimization (PSO) [25], genetic algorithm (GA) [26], Teaching and Learning Based Optimization (TLBO) [27].

GWO is a bionic optimization algorithm. It mimics the behavior of grey wolves to capture prey with a clear division of labor and mutual cooperation. At the top of the food chain, grey wolves mostly prefer to live in a pack [28]. Usually, there are 5–12 wolves in each group. They have a strict hierarchical management system that constitutes a hierarchical pyramid as shown in Fig. 3. This hierarchy allows the grey wolf pack to efficiently kill the prey. α layer is the head wolf, which is the strongest and most capable individual. It is also the only leader in a wolf pack, who directs the team’s predation actions, food distribution, and other decision-making tasks. β and δ layers are two wolves that are second only to α, their responsibility is mainly to assist α in the behavior of group organizations. ω is at the bottom of the pyramid, which occupies the majority of the total, and is mainly responsible for balancing the internal relationship of the population and looking after the young.

GW is well suited for the large search space and complex relationships of the EKF parameters. This GWO is used to optimize the performance of the EKF, which is represented by minimizing a fitness function shown in Figure 4. The fitness function takes an input in the form of a parameter set and uses the parameters in the EKF to estimate a trajectory. The corresponding position, velocity, and attitude ground truth solution for this trajectory is provided by a separate high-end INS/GNSS system, further described below. After the collection of both raw data and ground truth, the EKF tuning process is done offline. The difference between the EKF estimation and the known ground truth trajectory is used to produce the Root Mean Square Error (RMSE) of each state estimation. The RMSE of each state is then weighted and summed according to the equation in Figure 4, where the state errors are shown as east, north, and altitude in meters; and roll, pitch, and heading in degrees. The fitness function takes into account the scale differences between meters and radians by a separate weighting factor for each RMSE. The relative impact of the heading error is then compensated by a larger weight relative to the weights of the other errors. These weights are chosen through trial and error to achieve the best pose RMSE as determined by the users.

The process of the algorithm starts with generating a population of parameter sets uniformly distributed between bounds. The upper and lower bounds are empirically selected to leniently encompass all feasible values of the parameters, and the population is set to 100, chosen through trial and error. Each parameter set is evaluated by the fitness function and ranked according to fitness. A standard GWO and an example of the results is shown in Figure 5.

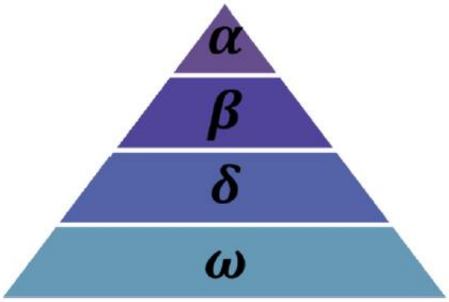

Fig. 3. Different grades of grey wolves.

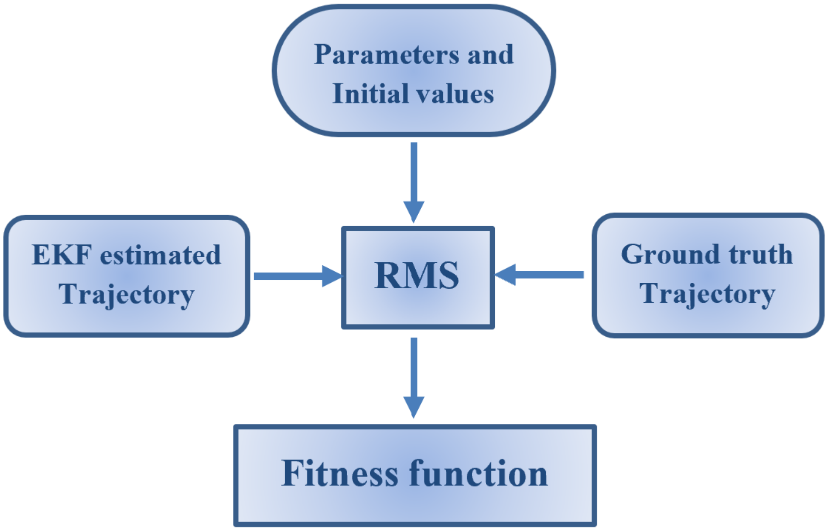

Fig. 4. Block diagram of fitness function.

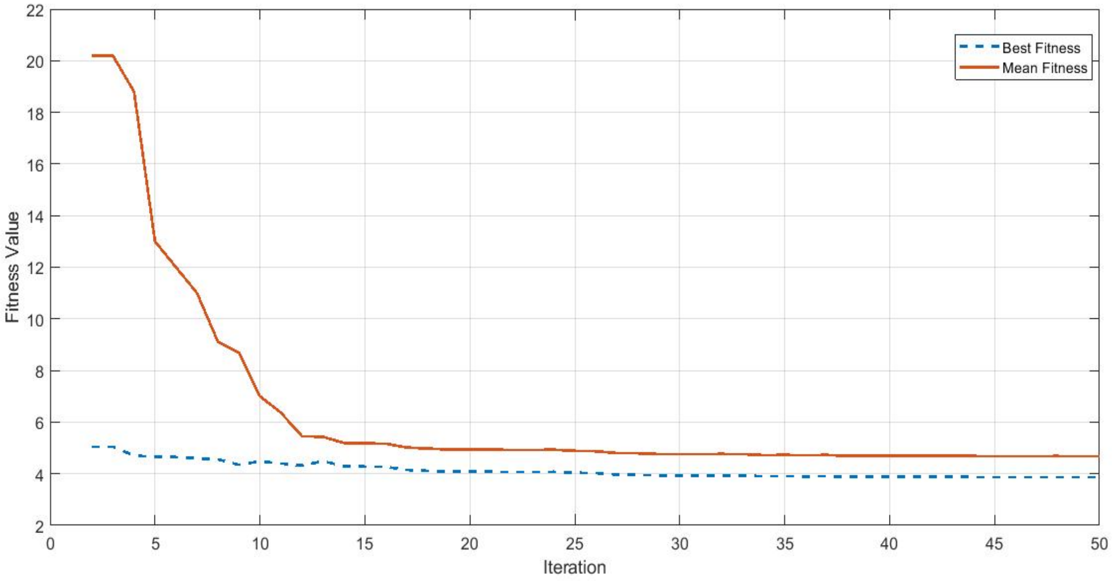

Fig. 5. Grey Wolf Optimization results.

Table 1. ***Nominal parameters.***

	GM Standard Deviation			GM Time Constant(s)			AV random Walk		
	x	**y**	**z**	**x**	**y**	**z**	**x**	**y**	**z**
Gyro(rad/s)	0.034	0.028	0.025	5194	4062	7439	0.13	0.14	0.14
Accel(m/s^2)	0.007	0.034	0.003	3619	103.32	6319	0.02	0.02	0.03

4. RESULTS

4.1 Nominal Design Point

First, GM and AV methods are applied to find the nominal design point. From the autocorrelation function of a 7-hour stationary IMU data recording, the GM bias time constants and standard deviations are calculated and displayed in Table 1. The AV random walk is also displayed in Table 1. For the rest of the parameters, values were tuned manually by trial and error over a few iterations.

4.2. Nominal and GWO Results

The above nominal values are then used with the EKF to estimate the trajectory. The performance results in RMSE are displayed in Table 2. The Grey wolf is then run to tune all parameters, where individuals are defined as sets of EKF parameters and wolves are individual parameters.

Using the m-file in MATLAB and Grey Wolf Algorithm Coding, with the population set to 100, the Grey wolf algorithm tuned EKF performed significantly better than that of the nominal EKF. In the results shown in Table 2, Grey wolf particularly improved the heading divergence that was produced by the nominally tuned EKF.

Table 2. ***RMSE result with Nominal and optimization Tuned parameters (Dataset 1).***

RMSE	Nominal Tuned parameters			Grey wolf Tuned parameters		
	Position(m)	**Velocity(m/s)**	**Orientation(deg)**	**Position(m)**	**Velocity(m/s)**	**Orientation(deg)**
East	0.86	0.32	0.59	0.59	0.08	0.38
North	2.20	0.66	0.51	0.51	0.11	0.13
Altitude	0.55	0.11	7.88	7.88	0.02	1.52

Table 3. ***RMSE Results for Datasets 1 and 2 with Grey wolf optimization.***

RMSE	Dataset2			Dataset3		
	Position(m)	**Velocity(m/s)**	**Orientation(deg)**	**Position(m)**	**Velocity(m/s)**	**Orientation(deg)**
East	0.06	0.05	0.27	0.09	0.09	0.29
North	0.11	0.10	0.14	0.08	0.09	0.61
Altitude	0.09	0.03	1.84	0.09	0.05	1.69

4.3. Filter Validation

EKF validation is done to confirm that the tuned parameters allow the EKF to properly model sensor characteristics and converge to accurate estimations for multiple trajectories that have not been used in the tuning and have not been seen by the filter before checking for over fitting. Using a GWO tuned parameter set, the performance results of an EKF estimation for two other trajectories are shown in this section. Three datasets named dataset 1, dataset 2, and dataset 3 were analyzed using Kalman filter without optimization and then using gray wolf optimization and localization accuracy was obtained which is given in the table below.

Table 3 shows the RMSE results of using tuned parameters in the EKF for test datasets 1 and 2. The parameters used have been tuned by the GWO on the tuning dataset only. The low error shows that the tuned EKF performs well for a variety of trajectories in addition to the dataset used to tune the parameters which verifies that there is no overfitting and the tuned filter can be used for other data sets that have not been used in the tuning process.

Table 3 shows the RMSE results of using tuned parameters in the EKF for 3 sets. The low error shows that the tuned EKF performs well for a variety of trajectories. In other words, path estimation using the gray wolf optimization algorithm is much more accurate than the conventional method.

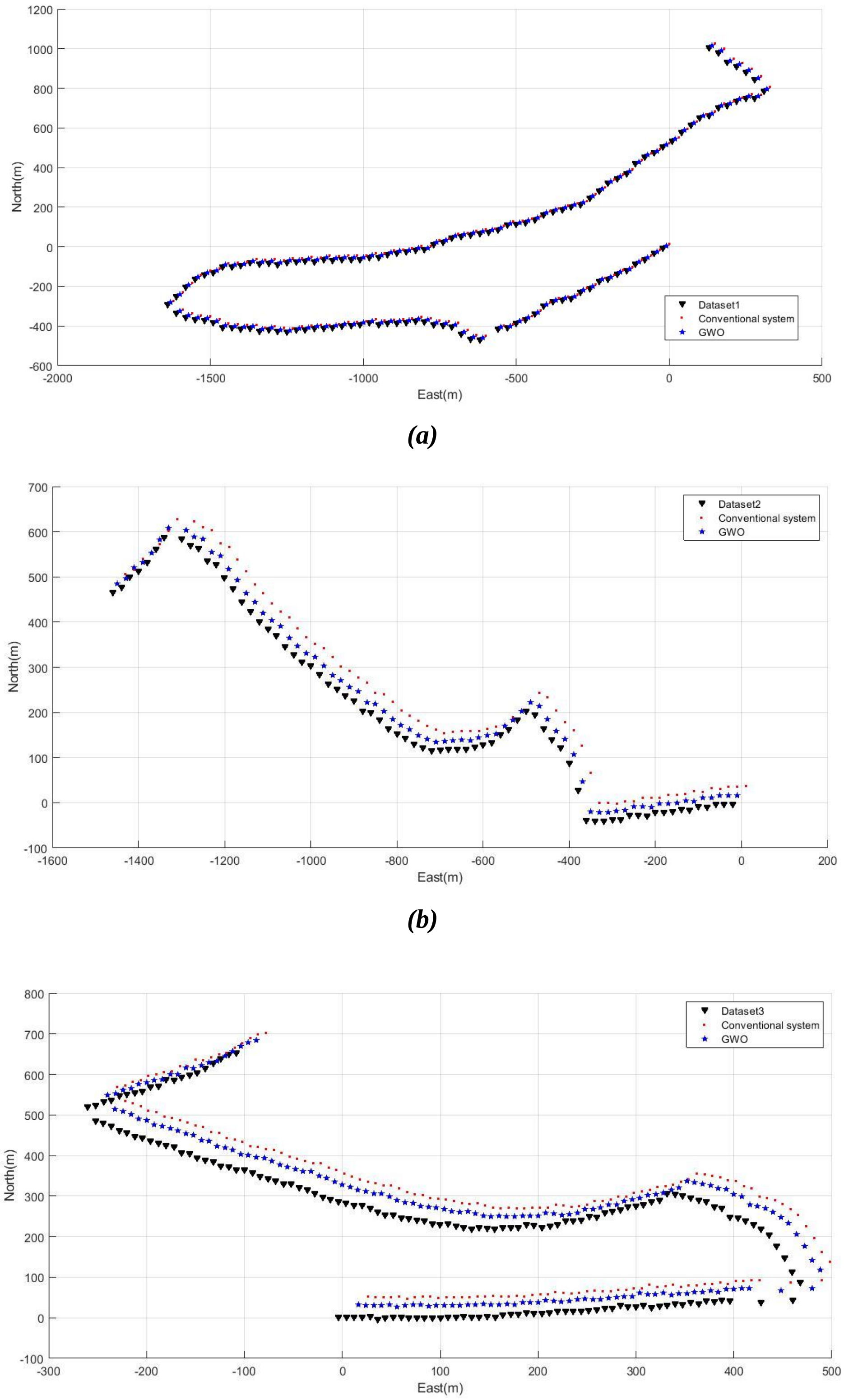

(a)

(b)

(c)

Fig. 6: Trajectories used and results.

5. Conclusion

In this paper, we tried to investigate the Indoor Vehicular Navigation using IMU and LiDAR and optimize the parameters of the Extended Kalman filter in this navigation system using the Grey Wolf optimization algorithm. To do this, the conventional IMU / LiDAR system was described and its mathematical relations were presented. Then, the Gray Wolf meta-heuristic algorithm was used to optimize its filter parameters. The results include comparisons between conventional and optimized IMU / LiDAR systems. It was shown that the application of meta-heuristic algorithm in optimizing the Kalman filter parameters can perform the navigation results of Indoor Vehicular Navigation more accurate. Therefore, for future work, it is suggested that the power of other meta-heuristic algorithms in vehicle navigation be examined and that other vehicle navigation systems be examined with this approach.

REFERENCES

[1] C. Cadena, L. Carlone, H. Carrillo, Y. Latif, D. Scaramuzza, J. Neira, I. Reid and J. J. Leonard, "Past, Present, and Future of Simultaneous Localization and Mapping: Toward the Robust-Perception Age," IEEE Transactions on Robotics, vol. 32, pp. 1309-1332, 2016.

[2] [U.S. Air Force, "Space Segment," National Coordination Office for Space-Based Positioning, Navigation, and Timing, 30 June 2020. [Online]. Available: https://www.gps.gov/systems/gps/space/. [Accessed 04 July 2020].

[3] M. Filipenko and I. Afanasyev, "Comparison of Various SLAM Systems for Mobile Robot in an Indoor Environment," in 9th IEEE International Conference on Intelligent Systems, Madeira, 2018.

[4] E. Yurtsever, J. Lambert, A. Carballo and K. Takeda, "A Survey of Autonomous Driving: Common Practices and Emerging Technologies," IEEE Access, vol. 8, pp. 58443-58469, 2020.

[5] W. Shao, S. Vijayarangan, C. Li and G. Kantor, "Stereo Visual Inertial LiDAR Simultaneous Localization and Mapping," arXiv preprint arXiv:1902.10741, 2019.

[6] Subakti, H.; Liang, H.-S.; Jiang, J.-R. Indoor Localization with Fingerprint Feature Extraction. In Proceedings of the IEEE Eurasia Conference on IOT, Communication and Engineering (ECICE 2020), Yunlin, Taiwan, 23–25 October 2020; pp. 239–242.

[7] X. Liu et al., "Kalman Filter-Based Data Fusion of Wi-Fi RTT and PDR for Indoor Localization," in IEEE Sensors Journal, vol. 21, no. 6, pp. 8479-8490, 15 March15, 2021, doi: 10.1109/JSEN.2021.3050456.

[8] Tiglao, N. M., Alipio, M., Dela Cruz, R., Bokhari, F., Rauf, S., & Khan, S. A. (2021). Smartphone-based indoor localization techniques: State-of-the-art and classification. Measurement, 179, 109349. doi:10.1016 / j.measurement. 2021.10.

[9] M. Kim, D. Han and J. -K. K. Rhee, "Multiview Variational Deep Learning With Application to Practical Indoor Localization," in IEEE Internet of Things Journal, vol. 8, no. 15, pp. 12375-12383, 1 Aug.1, 2021, doi: 10.1109/JIOT.2021.3063512.

[10] A. P, S. Z, N. A and E.-S. N, MEMS-Based INTEGRATED NAVIGATION, Norwood, MA: Artech House, 2010.

[11] M. Miroslav and Š. Mikuláš, "Computation and Evaluation Allan Variance Results," in 2016 New Trends in Signal Processing (NTSP), Demanovska Dolina, Slovakia, 2016.

[12] M. H. Elder, "MEMS IMU stochastic error modelling," Systems Science & Control Engineering, vol. 5, no. 1, pp. 1-8, 2016.

[13] Gulde, P., & Hermsdörfer, J. (2018). Smoothness Metrics in Complex Movement Tasks. Frontiers in Neurology, 9. doi:10.3389/fneur.2018.00615

[14] Figueiredo, A. I., Balbinot, G., Brauner, F. O., Schiavo, A., Baptista, R. R., Pagnussat, A. S., … Mestriner, R. G. (2020). SPARC Metrics Provide Mobility Smoothness Assessment in Oldest-Old With and Without a History of Falls: A Case Control Study. Frontiers in Physiology, 11. doi:10.3389/fphys.2020.00540

[15] Melendez-Calderon A, Shirota C and Balasubramanian S (2021) Estimating Movement Smoothness From Inertial Measurement Units. Front. Bioeng. Biotechnol. 8:558771. doi: 10.3389/fbioe.2020.558771

[16] Raj, T., Hashim, F. H., Huddin, A. B., Ibrahim, M. F., & Hussain, A. (2020). A Survey on LiDAR Scanning Mechanisms. Electronics, 9(5), 741. doi:10.3390/electronics9050741

[17] Wang, D., Watkins, C., & Xie, H. (2020). MEMS Mirrors for LiDAR: A Review. Micromachines, 11(5), 456. doi:10.3390/mi11050456

[18] Y. Li and J. Ibanez-Guzman, "Lidar for Autonomous Driving: The Principles, Challenges, and Trends for Automotive Lidar and Perception Systems," in IEEE Signal Processing Magazine, vol. 37, no. 4, pp. 50-61, July 2020, doi: 10.1109/MSP.2020.2973615.

[19] Niu, X., Yu, T., Tang, J., & Chang, L. (2017). An Online Solution of LiDAR Scan Matching Aided Inertial Navigation System for Indoor Mobile Mapping. Mobile Information Systems, 2017, 1–11.

[20] E.-H. Shin and E.-S. Naser, Accuracy Improvement of Low Cost INS/GPS for Land Applications, University of Calgary, Department of Geomatics Engineering, Calgary, Canada, 2001, 2001.

[21] [21] E. H. Shin, Estimation Techniques for Low-Cost Inertial Navigation UCGE report, 20219, 2005,

[22] M.G. Gong, L.C. Jiao, D.D. Yang, et al., Research on evolutionary multi-objective optimization algorithms, J. Softw. 20 (2009) 271–289.

[23] I. Rechenberg, Evolutionsstrategie Optimierung technischer Systeme nach Prinzipien der biologischen Evolution, 15, 1973.

[24] X.S. Yang, Nature -I nspired

Metaheuristic Algorithms, Luniver Press, 2008.

[25] J. Kennedy, R. Eberhart, Particle swarm optimization, in: International Conference on Neural Networks, vol. 4, IEEE, 2002.

[26] D.E. Goldberg, Genetic Algorithms in Search, Optimization & Machinelearning, 1989.

[27] A. Mortazavi, V. Toğan, A. Nuhoğlu, Interactive search algorithm: A new hybrid metaheuristic optimization algorithm, Eng. Appl. Artif. Intell. 71 (2018) 275–292.

[28] [S. Mirjalili, S.M. Mirjalili, A. Lewis, Grey Wolf Optimizer, Adv. Eng. Softw. 69 (2014) 46–61.